

Study of CMOS APS Responsivity Enhancement: Ring-Shaped Photodiode

Tatiana Danov, Igor Shcherback, Orly Yadid-Pecht, *Senior Member, IEEE*

The VLSI Systems Center
Ben Gurion University
P.O.B. 653 Beer-Sheva 84105, ISRAEL
TEL: 972-8-646152; Fax: 972-8-6477620
E-Mail: oyp@ee.bgu.ac.il

ABSTRACT

In this work the possibilities of CMOS APS spectral response improvement are discussed. Thorough submicron scanning results obtained from various ring-shaped pixel photodiodes with different inner radius, implemented in a standard CMOS 0.35 μ m technology, are compared with numerical computer simulations. The functional dependence of the pixel response on the ring opening size was discovered and formulated for various wavelengths illumination. We show that the photodiodes with a small ring-opening exhibit better sensitivity in the blue spectrum range (420-460 nm). Comparison between the simulation and measurement results shows a good agreement, hence proving that specific photodiode designs enable to selectively improve pixel color sensitivity.

Index Terms - APS (Active Pixel Sensor), CMOS image sensor, minority carriers, diffusion, photocurrent, sensitivity.

I. INTRODUCTION

Nowadays, CMOS based imagers offer significant advantages over CCDs such as low voltage, low power consumption, lower cost [1]. At this time of CMOS technology rapid downscale, small pixel size, low dark current, high fill factor, and low noise are required for high-resolution imagers. Increasing sensitivity with the available CMOS structures, comparable to these of CCDs, is still one of the major manufacturers' problems. Various specialized devices and materials have been developed to increase the sensitivity without much payment in pixel area [2]-[5]. An analysis of the pixel design effect on the APS responsivity was performed in [6]-[8]. In this paper, we investigate the influence of the ring-shaped photodiode design on APS sensitivity, and show how to enhance the device sensitivity to short wavelengths illumination, i.e. to blue light. The opto-electrical characteristics of the ring-structures are described in Sections 2-3.

II. SIMULATION RESULTS

2.1 Background

Photon absorption in silicon depends on the wavelength dependant absorption coefficient $\alpha(\lambda)$. The collection of the photogenerated carriers depends on the carrier absorption depth, $L_{opt}=1/\alpha$, lifetime (τ_n or τ_p), and the characteristic diffusion length (L_n or L_p). Perfect collection efficiency is assumed for the electron-hole pairs generated within the device depletion region. Carriers generated outside the depletion region may be collected as they might diffuse into the depletion region.

Red light, with wavelength, $\lambda\sim 0.6\mu m$ for instance, has a relatively small absorption coefficient, which means more of the photocarriers can be generated outside the depletion

region (p-type substrate in our case). These carriers diffuse to the original imaging site or to a nearby site where they are collected, before they are lost to the bulk recombination process. The imagers lose resolution as the result of this diffusion process.

"Blue" photons, e.g., with $\lambda \sim 0.4 \mu m$, tend to be absorbed near the device surface (into the N^+ region in our case). The high doping density in this region strongly reduces the carrier lifetime, such that most of the minority carriers recombine immediately; causing therefore low photodiode sensitivity for short wavelengths illumination.

2.2 Electrooptical Characteristics Simulation

We have investigated the photoresponse in CMOS ring-shaped photodiodes by means of numerical device simulations for different wavelength illuminations (covering the visible spectrum, 420-700 nm). The simulator used is *MediciTM* [9] and it solves the Poisson's and the continuity equations. Ring-shaped N^+/P -Well photosensitive elements with different inner-ring-radiuses (i.e., 0.2 μm , 0.25 μm , 0.35 μm , 0.5 μm , and 0.6 μm) were investigated. Note that all simulations are based on the parameters reported for the standard CMOS 0.35- μm technology process. The simulation results are compared with the results obtained by thorough scanning of various ring-shaped photodiode APS fabricated in standard 0.35 μm CMOS technology. Note that the illumination spot size and photon flux were kept constant (for each λ) in order to simplify the results comparison.

Fig. 1 shows the normalized output signal distribution obtained from different inner-radius photodiodes as a function of the illumination spot position. It is possible to see that the photosignal from the ring-opening decreases as the ring-radius increases (the normalized photosignal varies from 0.67 for $r_{inner}=0.6 \mu m$, to 0.97 for $r_{inner} =0.2 \mu m$), while the signal magnitude from the active-ring part remains unaltered (the normalized photosignal is ≈ 1).

Fig. 2 presents an example of the normalized photosignal versus light spot position, obtained for the particular photodiode (with $r_{inner}=0.25\mu m$), and with different wavelengths. The diode reveals the intensified response in the blue region (420-460 nm), i.e., the photosignal from the ring-opening region is higher than from the active part of the diode.

Fig. 3 represents the simulation results obtained for several ring photodiodes in the blue spectral diapason ($\lambda \leq 460$ nm). The photoresponse obtained from the ring-opening is compared with the corresponding active-part response (the N^+ part photoresponse, which is indicated by the dashed line). It is possible to see that the diodes with a small opening-radius exhibit higher sensitivity in comparison to diodes illuminated in the active area, i.e., the “blue” signal from the “window” stays higher than the "blue" signal from the ring itself, in all the range from 420 nm to 460 nm. Note that the “window” dominance reduces with wavelength increase, such that the difference between the “window” and ring-part signals varies from 8% for 420 nm to 3.8 % for 460 nm.

III. COMPARISON WITH EXPERIMENTAL RESULTS AND DISCUSSION

In order to check the presented simulation results we have performed experimental investigations by means of the unique sub-micron scanning system (S-cube system) reported before [10]- [11], which enables a detailed, point by point, quantitative determination of the contributions to the total output signal from each particular region of the pixel in a resolution suitable for today’s advanced technologies (sub-micron). A set of various ring-shaped $7\mu m$ -pitch pixels (see Fig. 4 for a layout example) fabricated in standard CMOS $0.35\mu m$ technology was thoroughly scanned in several wavelengths illumination.

Fig. 5 shows an example of the responsivity map obtained for $\lambda=454nm$ by thorough sub-micron scanning for a ring- shaped pixel illustrated in Fig. 4.

Two lines in Fig. 6 corroborate the simulation results and present the averaged responsivity maps cross-section through the photodiode center for $\lambda=454nm$ (the solid line in Fig. 6) and $\lambda=632nm$ (the dashed line in Fig. 6), corresponding to Figs. 4 and 5. In Fig. 6 the response for $\lambda=632nm$ is “flat”, while for $\lambda=454nm$ the photosignal from the “window” region (region "A") is higher than in the active part (regions "B" and "C", where the difference between the "blue" signals from regions "A" and "B" or "C" is estimated to be 26%).

It is possible to understand and explain this effect with regard to the absorption mechanism in silicon. We consider analytically the excess minority carrier behavior separately in two regions, i.e., within the ring itself and in the “window” opening. The continuity equation for holes (in the ring photodiode region) or electrons (in the ring-opening region) is:

$$\frac{\partial^2 p(y)}{\partial y^2} - \frac{p(y)}{L_p^2} + \frac{G_0}{D_p} \exp\left(-\frac{y}{L_{opt}}\right) = 0 \quad (1)$$

where G_0 is the photogeneration rate at the surface, D_p is the diffusion coefficient, L_p is the holes diffusion length, $L_p = \sqrt{D_p \tau_p}$, τ_p is the holes lifetime, and L_{opt} is the light absorption depth.

For depth $0 \leq y \leq y_{junction}$, where $y_{junction}$ is the photodiodes junction depth (see Fig.7) the solution for holes:

$$p(y) = \frac{A}{\sinh\left(\frac{y_{junction}}{L_p}\right)} \left(e^{-y_{junction}/L_{opt}} \sinh\left(\frac{y}{L_p}\right) - \frac{L_p^2}{L_{opt}^2} \sinh\left(\frac{y - y_{junction}}{L_p}\right) \right) - A e^{-y/L_{opt}} \quad (2)$$

with $A = \frac{G_0 L_{opt}^2 L_p^2}{D_p (L_p^2 - L_{opt}^2)}$, and satisfying the following boundary

conditions: $\left. \frac{\partial p(y)}{\partial y} \right|_{y=0} \rightarrow \max$, and consequently $\frac{\partial^2 p(y)}{\partial y^2} = 0$ (since light is strongly absorbed

in the thin surface layer, where the doping level is high, and the photogeneration rate is

maximum (e.g., equal to G_0 at the surface); in this region the surface recombination for "blue" photoelectrons can be neglected [12]), and $p(y) = 0$, $y = y_{junction}$.

The boundary conditions for excess minority electrons in the ring-opening are as follows:

$$\left. \frac{\partial n(y)}{\partial y} \right|_{y=0} \rightarrow \max; \Rightarrow \frac{\partial^2 n(y)}{\partial y^2} = 0, \quad \text{and} \quad \left. \frac{\partial n(y)}{\partial y} \right|_{y \gg L_{opt}} = 0, \quad \text{i.e., the concentration gradient}$$

eventually decreases to zero far beyond the absorption depth. Subject to these boundary conditions, the solution for photoelectrons, is

$$n(y) = A \frac{L_n^2}{L_{opt}^2} e^{-\frac{y}{L_n}} - A e^{-\frac{y}{L_{opt}}} \quad (3)$$

Assuming planar X-Z symmetry, we consider the one-dimensional continuity equation in the X-direction:

$$\frac{\partial^2 p(x)}{\partial x^2} - \frac{p(x)}{L_p^2} + \frac{G_0}{D_p} e^{-\frac{y}{L_{opt}}} = 0, \quad (4)$$

having the solution

$$p(x) = p(y) e^{-\frac{x}{L_p}} - B e^{-\frac{y}{L_{opt}}} (e^{-\frac{x}{L_p}} - 1), \quad \text{where} \quad B = \frac{G_0 L_p^2}{D_p} \quad (5)$$

satisfying the boundary conditions: $p(x=0) = p(y)$, where $x=0$ is the light hitting point

within the pixel, and $\left. \frac{\partial p(x)}{\partial x} \right|_{x \gg L_p} = 0$, describing that the minority carrier concentration

approaches equilibrium value at the length far beyond the diffusion length, therefore the concentration gradient turns to zero. This distribution for $\lambda=420\text{nm}$ is presented in Fig. 8 (a).

The solution for the photoelectrons, obtained in the same way, is

$$n(x) = n(y) e^{\frac{x}{L_n} - B} e^{-\frac{y}{L_{opt}}} (e^{\frac{x}{L_n}} - 1) \quad (6)$$

This distribution for $\lambda=420\text{nm}$ is presented in Fig. 8 (b).

The complete photocurrent rises because of the diffusion photocurrent via the sidewall and the bottom facets of the depletion region; and the drift photocurrent caused by the photocarriers generated and collected directly in the depletion region.

The photocurrent estimation for short wavelengths illumination (approximately $\leq 420 \text{ nm}$) can be calculated with regard to the sidewall and bottom collection areas, i.e., we can take into account the diffusion current only. The drift current calculation shows that we can

neglect the "blue" drift current $\left(\frac{J_{diff}}{J_{drift}} \right)_{\lambda=420nm} \approx 10$).

Figs.8 (a, b) demonstrate the planar minority carrier distribution (X- direction).

In Fig. 8 (a) the excess minority holes concentration approaches the equilibrium value at the distance of $x \sim 0.35 \mu\text{m}$, while the excess minority electrons concentration turns to its quasi-constant value at the length far beyond $x \sim 5 \mu\text{m}$ (Fig. 8 (b)).

The diffusion photocurrent that is collected through the sidewalls and the bottom of the depletion region [8] is obtained therefore as follows;

Ring photodiode:

$$I_{diff} = \int_0^{y_{junction}} J_p(x) P dy + J_p(y) \Big|_{(at y=y_{junction})} S_{bottom}, \text{ where } P \text{ is the sidewall perimeter, and}$$

$$J_p(x) = -qD_p \frac{\partial p(x)}{\partial x}, \quad J_p(y) = -qD_p \frac{\partial p(y)}{\partial y} \quad (7)$$

Ring-opening region:

$$I_{diff} = \int_0^{y_{junction}} J_n(x) 2\pi R dy$$

, where $J_n(x)$ is the diffusion electrons current density, i.e.,

$$J_n(x) = qD_n \frac{\partial n(x)}{\partial x}$$

and R is inner ring radius. (8)

We have calculated (using equations (7)-(8)) and compared the complete diffusion photocurrent in two different regions (ring-opening and ring-photodiode)

$$\left(\frac{I_{diff}^{ring-opening}}{I_{diff}^{ring-itself}} \right)_{\lambda=420nm} \approx 1.49$$

The absorption depth for “blue” photons is a few tenths of micrometers, i.e., most of the potential contributors are created close to the surface and should be absorbed before they are lost in recombination. The ring-shaped photodiode architecture evolved mainly due to this basic requirement: the depletion region (which has two collection areas: bottom and sidewall collection areas [8]) should be spaced close to the surface. The peculiarity of the silicon interaction with the blue light allows to assert that the sidewall collection area of the depletion region becomes dominant for "blue" photocarriers collection. Moreover, keeping in mind the scaling tendencies, i.e., the shallower depletion and more highly doped regions, this requirement becomes more significant [13].

The ring photodiode architecture enables its sidewall collection region enlargement. Blue photocarriers created within the ring-opening, diffuse quickly towards the very closely set sidewall depletion, since they are surrounded by a sidewall of the space charge region.

Moreover, the photocarrier creation can occur within the depletion sidewall itself and directly contribute to the signal. The schematic illustration of this process is shown in Fig.7. Therefore, the excess “blue” carriers loss decreases, the photoelectron collection efficiency of the photodiode increases, and pixel electrical signal increases. Note that most of the “red” contributors are collected through the bottom depletion collecting surface, since they are generated in the deep substrate (5-8 μm) and then diffuse in all directions.

IV. SUMMARY

In this work, an investigation of a ring-shaped photodiode CMOS APS has been presented. The simulation and experimental results obtained from different inner-radius photodiodes present pixel sensitivity improvement in the “blue” spectral region. This property of pixel photodiode was discovered in diodes with a relatively small opening size, clearing therefore the way for further investigation in more advanced CMOS technologies. Moreover, the presented results determine the line for further improvement and for “intelligent” design optimization, enabling the required optical response and the desirable color differentiation.

V. REFERENCES

- [1] O. Yadid-Pecht and Ralph Etienne-Cummings (Eds.), "CMOS IMAGERS: FROM PHOTOTRANSDUCTION TO IMAGE PROCESSING," Kluwer academic publishers, spring 2004.
- [2] B. C. Burkley *et al.*, "The pinned photodiode for an interline-transfer CCD image sensor," in *IEDM Tech. Dig.*, pp. 28-31, Dec. 1984.
- [3] S. Manabe *et al.*, "A 2-million-pixel CCD image sensor overlaid with an amorphous Silicon photoconversion layer," *IEEE Trans. Electron Devices*, vol. 38, pp.1765-1771, Aug. 1991.
- [4] S. Mendis, S. Kemeny, and E.R. Fossum, "A 128x128 CMOS active pixel image sensor for highly integrated imaging systems," in *IEDM Tech. Dig.*, pp. 583, 1993.
- [5] T. Lule S. Benthien, H. Keller, et al., "Sensitivity of CMOS Based Imagers and Scalling Perspectives," *IEEE Trans. Electron Devices*, vol. 47, pp.2107-2122, Nov. 2000.
- [6] O. Yadid-Pecht, B. Mansoorian, E. Fossum, B. Pain, "Optimization of active pixel sensor noise and responsivity for scientific applications", *Proc. SPIE/IS&T Sym. on Electronic Imaging: Science and Technology*, San Jose, California, Feb 10-13, 1997.
- [7] J. S. Lee, R. I. Hornsey, "CMOS Photodiodes with Substrate Openings for Higher Conversion Gain in Active Pixel Sensors," *2001 IEEE Workshop on CCDs and Advanced Image Sensors*, Crystal Bay, Nevada, June 2001.
- [8] I. Shcherback and O. Yadid-Pecht, Chapter 3, in "CMOS IMAGERS: FROM PHOTOTRANSDUCTION TO IMAGE PROCESSING," O. Yadid-Pecht and Ralph Etienne-Cummings (Eds.), Kluwer academic publishers, spring 2004.
- [9] Avant! Corporation, Medici 4.1 User's Manual, Fremont, CA, July 1998.
- [10] I. Shcherback, O. Yadid-Pecht, "CMOS APS Crosstalk Characterization Via a Unique Submicron Scanning System," *IEEE Trans. Electron Devices*, Vol. 50, No. 9, pp.1994-1997, Sept. 2003.
- [11] I. Shcherback, B. Belotserkovsky, O. Yadid-Pecht, "A Unique Sub-micron Scanning System use for CMOS APS crosstalk characterization , " in *Proc. SPIE on Sensors, Cameras and Systems for Scientific/Industrial Applications*, Vol. 5017, pp 136-147, San Jose, California USA, 22-23 January, 2003.
- [12] S.G.Chamberlain, et al., "Spectral Response Limitation Mechanisms of a Shallow Junction $n^+ -p$ Photodiode", *IEEE Journal of Solid-State Circuits*, Vol. Sc-13, No. 1, pp. 167-172, February 1978.
- [13] I. Shcherback, O. Yadid-Pecht, "Prediction of CMOS APS Design Enabling Maximum Photoresponse for Scalable CMOS Technologies," *IEEE Trans. Electron Devices*, Vol. 51, No. 2, pp. 279- 282, Feb. 2004.

LIST OF FIGURES

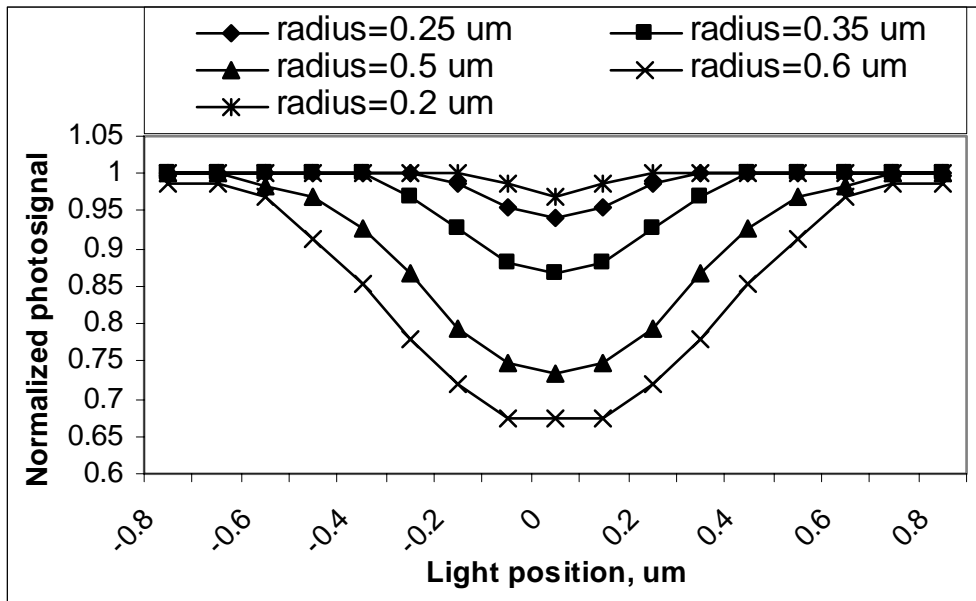


Fig. 1: The normalized output signal distribution obtained from different inner-radius photodiodes as a function of the illuminating spot position ($\lambda=632 \text{ nm}$). The point of $0 \mu\text{m}$ corresponds to the ring center of the photodiode.

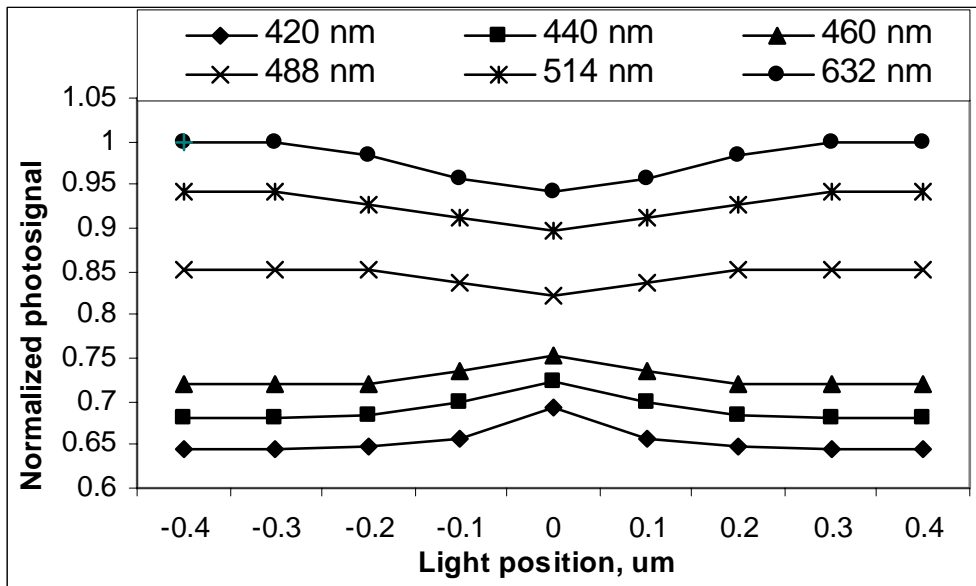


Fig. 2: Example of the normalized electrical signal simulated for the diode with inner radius of $0.25 \mu\text{m}$. The characteristics are obtained for the visible range (420-632 nm). The point of $0 \mu\text{m}$ corresponds to the ring center of the photodiode.

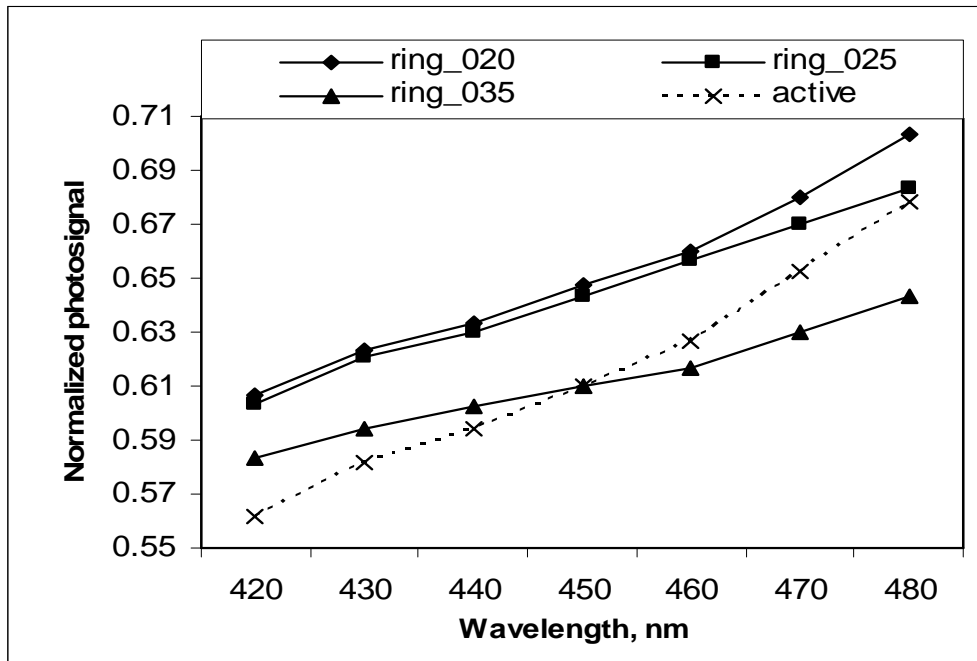


Fig. 3: The pixel sensitivity characteristics, simulated for several ring photodiodes (with a small inner radius), in the blue spectral diapason. The dashed line demonstrates the photosignal corresponding to the diode active part illumination (ring-photodiode region); the solid lines correspond to the “window” lighting (ring-opening region). The influence of the ring-opening radius is clearly emphasized, such that smaller radius gives rise to better response.

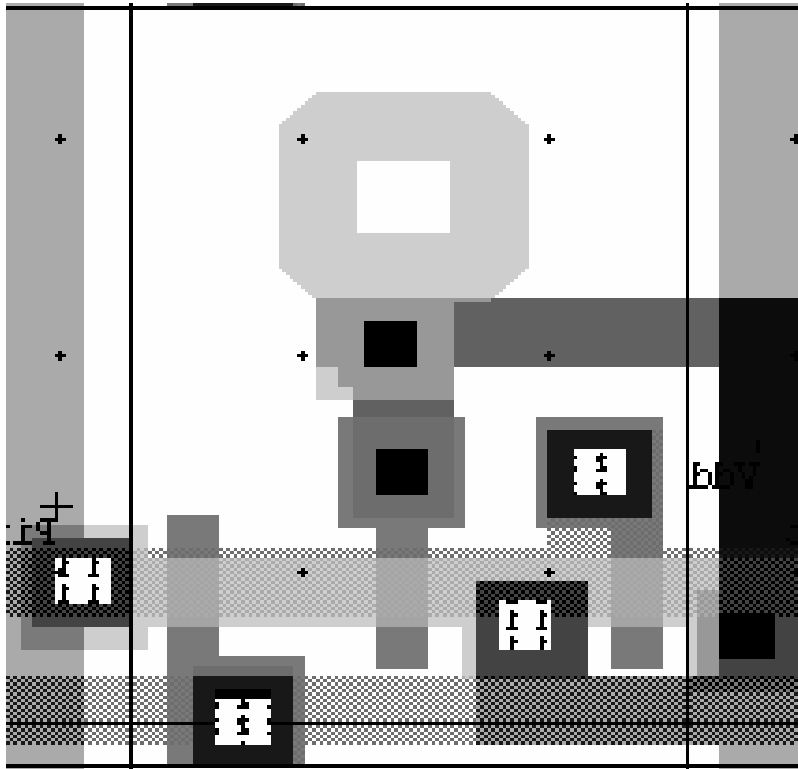


Fig. 4: A design layout example of a ring-shaped active area pixel with inner photodiode radius of $0.4 \mu\text{m}$, and active layer (ring) width of $0.6 \mu\text{m}$.

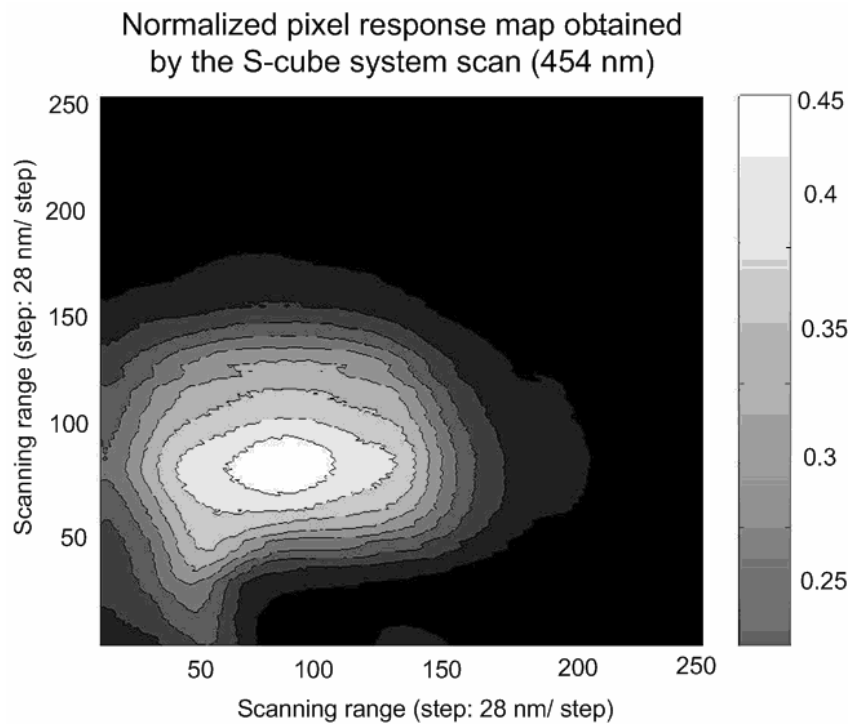


Fig. 5: The pixel normalized response map example obtained by the S-cube system scan (454 nm) in correspondence to Fig. 4.

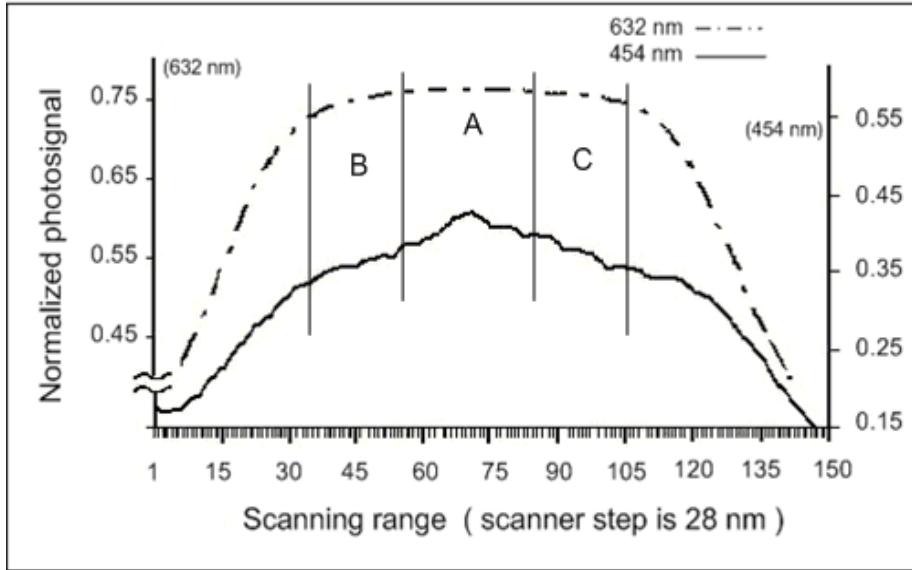


Fig. 6: The averaged responsivity maps cross-section through the photodiode center for $\lambda=454 \text{ nm}$ (the solid line) and $\lambda=632 \text{ nm}$ (the dashed line) corresponding to Figs. 4 and 5. The response for $\lambda=632 \text{ nm}$ is “flat”, while for $\lambda=454 \text{ nm}$ the photosignal from the “window” region (region "A") is higher than in the active part (regions "B" and "C", where the difference between "blue" signals from regions "A" and "B" or "C" is estimated to be 26%).

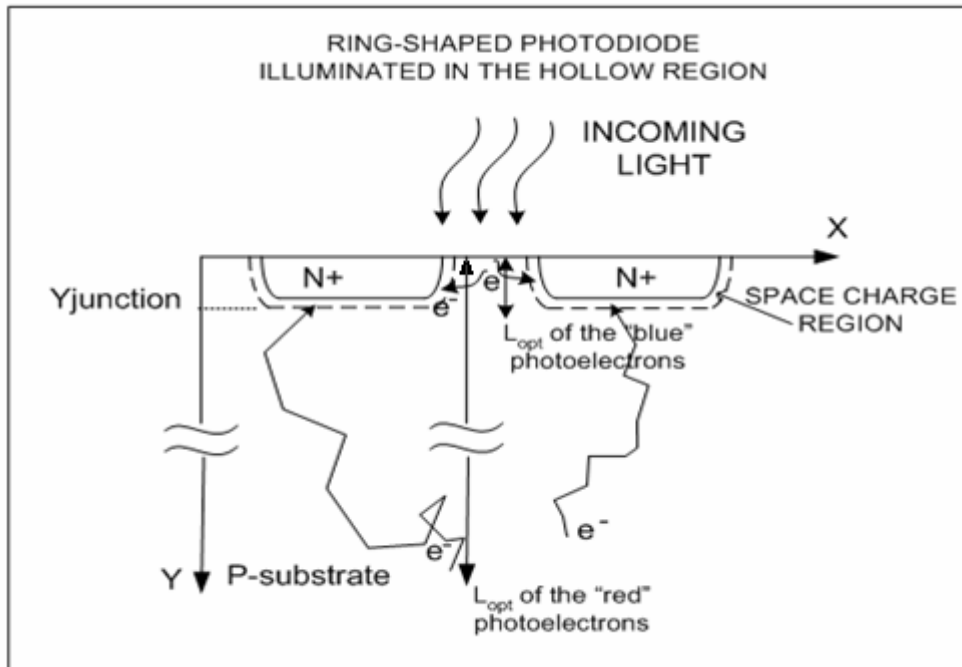
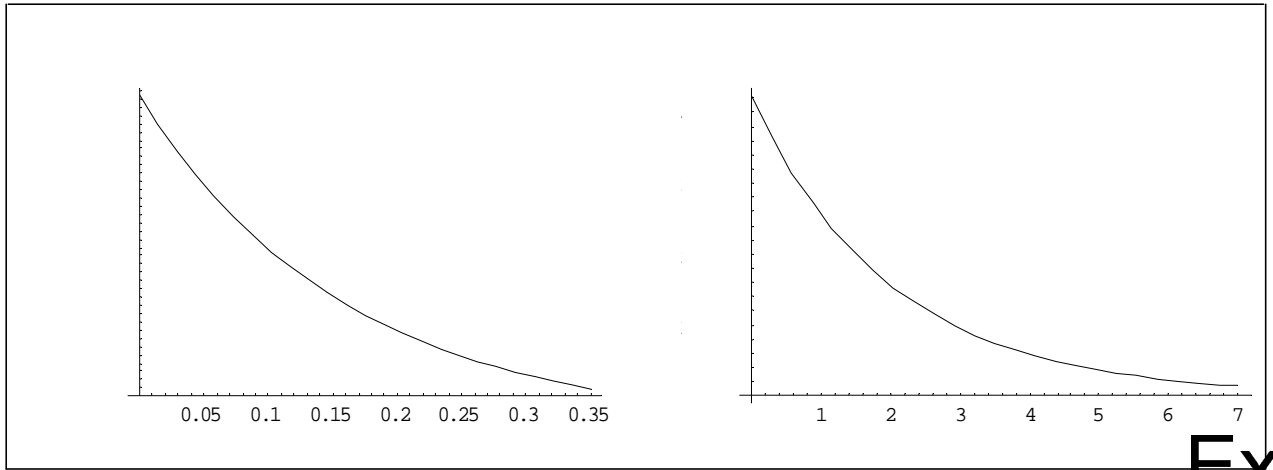


Fig. 7: Schematic cross section of the ring-diode through its center. The difference between the “blue” and the “red” photons absorption mechanisms is indicated regarding different absorption depths, i.e., $L_{opt}^{red} \gg L_{opt}^{blue}$.



Exce

Fig.8: Minority photocarriers planar distribution (X-direction): (a) - for holes in ring-photodiode region, and (b)- for electrons in ring opening region, after $\lambda=420nm$ light illumination. The excess minority holes concentration (region (a)) approaches a quasi-constant value at the distance x about $0.35 \mu m$, whereas the excess minority electrons concentration (region (b)) narrows at the length far beyond $4.5 \mu m$.

Normalized concentration, $10^{-14} / cm^3$

13.75

13.50

13.25

13.00